Mo P18

Image Based Pore-scale Models of Flow through Porous Media - Oil Recovery Applications

I.I. Bogdanov* (ADERA), J. Kpahou (University of Pau) & I. Bondino (Total SA)

SUMMARY

The importance of pore-scale flow models for practical applications is widely recognized. Due to recent advances in computed microtomography (μCT) the reconstructed samples are now used for direct numerical simulations (DNS) of the flow. This technique gives a unique opportunity for non-destructive characterization; nevertheless a typical study encounters several challenges. The discussion of the most difficult steps of modeling methodology is our first objective.

The description of dynamic phase distribution and behavior of the fluid interface is a problem of primary importance. A regularization technique may affect the results in non-trivial ways; instead the diffuse-interface method offers a thermodynamic description of phase “mixing” zone and handles the morphological changes of interface and related physical effects. A series of model tests including the juxtaposition to analytical solutions for capillary channel flow, estimation of spurious velocity around a droplet and others, are presented. The quantitative demonstration of the method is our second objective.

Among numerous oil recovery applications one can mention the transport properties determination for different physical environment, the study of fluids entrapment/mobilization, the flow patterns at different capillary numbers and viscosity ratios, the emulsion and foamy oil flow, etc. Here we address the analysis of viscous fingering dynamics (oil-water systems, 2D synthetic medium) and the 3D stationary configurations of single and two-phase flow in real porous samples at different Reynolds, Cahn and capillary numbers. In particular, the computations based on μCT image reconstruction aims at the examination of fluid irreducible saturations. This constitutes our third objective. A discussion on the possibilities and limits of the model in quantitative characterization of porous materials is offered. Contribution of the pore-scale DNS to reservoir characterization becomes an increasingly important factor for numerous practical oil recovery applications.

Introduction

During the last decades the importance of pore-scale flow models for petroleum and environmental applications has been widely recognized. The fast and continuous development of technical basis for computations and pore-scale measurement and visualization is giving rise to problem formulations which seemed inappropriate even in the relatively recent past. A straightforward illustration is represented by the direct numerical simulations (DNS) technique of flow through porous media (PM). During long enough time direct pore-scale modelling (PSM) was considered senseless and/or impossible because the flow fields could not be reliably observed and measured at this scale (cf. Bear 1988, chapter 1) and thus could not provide any meaningful information for model building. It makes no sense to argue that during decades that was true. However, currently micro-tomography and microscope imaging are becoming common techniques and numerical simulations coupled with laboratory measurements can now address the pore-scale phenomena description getting back to a fundamental approach in hydrodynamics (cf. Adler et al. 1990, Fourie et al. 2007). The direct pore-scale flow analysis is gaining growing interest as an increasingly important domain in porous medium research.

The main objective of the PSM based on a DNS approach is the determination of dynamic fluids distribution and their behaviour inside a "real" pore volume. Therefore the precise geometrical characterization of void space in natural materials becomes a first key issue. Here the X-ray computed micro-tomography (μCT) technique gives a unique opportunity for non-destructive 3D core sample insight (cf. Wildenschild and Sheppard 2013). The description of a physical interface separating fluid phases is another problem of crucial importance for such a modeling. Instead of using a regularization technique aimed at capturing the interface, the diffuse interface (DI) method is based on thermodynamic treatment of phase transition (or phase mixing) zone using any intensive scalar property of a system (*eg.* a component molar density for binary systems, Cahn and Hilliard 1958). As a result, it is a good choice for a numerical technique, handling the morphological changes of the interface (Jacqmin 1999).

So the numerical methodology under consideration includes the geometrical description of flow regions based on μCT imaging, the generation of a 3D grid in a real pore space, the application of adequate discretized numerical models and the robust flow calculations using solvers of high computational performance (cf. Bogdanov et al. 2012). To build, test and validate the relevant model for DNS of pore-scale flow in real media geometry under natural flow conditions is our primary objective.

Hereinafter we will use the term "pore-scale" and not "micro-scale" to respect the notion of "microscopic point" defined to refer a representative elementary volume (REV) scale containing, by definition, numerous pores (cf. Bear 1988) and to distinguish between it and the geometries under consideration. This just means that currently one of the principal objectives of our modelling is *to approach* the REV scale description.

Numerous oil recovery applications can be mentioned even within this relatively simple physical framework including first of all the single (1P) and two-phase (2P) transport properties determination in the real sample environment, the investigation into fluids entrapment and mobilization, the pore-scale flow patterns at different viscosity ratios, the emulsification and its consequences, the foamy oil flow, etc. Here we address the analysis of viscous fingering dynamics (oil-water systems, 2D synthetic medium) and the 3D stationary configurations of single and two-phase flow in real porous samples at different transport and capillary conditions. In particular, the computations based on μCT image reconstruction were focused on the examination of the two-phase flow stationary configurations. The desaturation followed the imbibition end-point saturations are presented and discussed.

All computations presented below have been performed on slightly different PC configurations which included Intel Xeon E5-2690 CPU (or close) using parallel computations on less than 8 cores (typically from 4 to 6 cores).

Model of a real medium: images preparation and processing

The range of energies used in the X-ray tomography allows a study of dense objects, for example, such as rocks, of centimetric size; moreover, the μCT technique gives a unique opportunity for non-destructive 3D core sample insight. Typically the image stack generation is done step by step, the most important of them being briefly described below.
The acquisition: for our study, a tomography device, Skyscan 1172 μCT (by Brucker microCT, Figure 1), is used to analyse rock samples. A well referenced rock, the *Bentheimer* sandstone, has been investigated. For this a cylindrical 8 mm thick in diameter, 20 mm long plug of this sandstone is shaped and fixed inside the analysis chamber. The main result of this step is a stack of images composed of 500 slices of 500×500 pixels each; this stack is read as a 500^3 voxels virtual 3D rock sample. With a 4.9 μm resolution, about 14.7 mm3 is thus investigated for this study. Finally the linear size of image based sample geometry was L=2.45 mm.
The pre-processing: prior to measuring object's properties and extracting accurately the inner geometry, an image processing is required to improve the signal/noise ratio as the volume is still coarse (composed of raw, noisy images). Then, the result is segmented to separate porosities from the bulk (image binarization).
The geometrical description: the procedure described above cannot prevent the binarized stack from artefacts, due to inaccuracy of the segmentation process. If these artefacts have no impact on the sample transport properties, they can be removed. Note that if the volume is not processed to get rid of these elements, the geometry of the object will be too much time and memory consuming for calculations. To reduce the total number of voxels involved, a data *resampling* and/or volume *cropping* can be applied (using *eg.* ScanIP by SimpleWare). Isotropic *resampling* does not modify an object in size but reduced significantly the total number of voxels. This operation may be somewhat critical because it modifies the connectivity, and hence the transport properties (for example, weakly linked connections between pores may be removed etc.). The *cropping* is used to choose a subregion of interest in size and location, inside the stack. This cutting process can isolate some porous areas from the main network (indeed, new boundaries are generated), so the main network has to be extracted from the new volume, and the unconnected porosity removed.
Mention finally that for uncompressible flow modelling only the grain surface reconstruction is necessary to reproduce and mesh the pore volume of the rock sample.

Figure 1 *Laboratory setup with the Skyscan 1172 microtomograph and the Bentheimer sample inside.*

Diffuse interface approach

Governing equations

Only the brief description of the diffuse interface method and its underlying ideas is presented here. For more details of the theory and its formalism see *eg.* Jacqmin (1999), Badalassi et al. (2003), Fichot et al. (2007). The second gradient theory assumes that free energy of a system is a functional of an order parameter φ, its gradient $\nabla\varphi$ and the temperature T:

$$F = F(\varphi, \nabla\varphi, T) \tag{1}$$

In the case of an isothermal binary fluid, a free energy can be defined for flow configurations where the system is not in equilibrium as:

$$F(\varphi, \nabla\varphi) = \alpha \int_{\Omega} f \, dV = \alpha \int_{\Omega} \frac{1}{2}\left(|\nabla\varphi|^2 + g(\varphi)\right) dV \tag{2}$$

where Ω is the region of space occupied by the system and φ (the dimensionless order parameter or the phase-field variable) serves to identify the two fluids with volume fraction $(1+\varphi)/2$ and $(1-\varphi)/2$. The chemical potential is defined as:

$$\nu = \alpha \, f'_{\varphi}, \tag{3}$$

where α is the mixing energy density. For $g(\varphi)$ a following double potential form with minima at $\varphi=\pm1$ indicating two immiscible phases, can be chosen:

$$g(\varphi)=(1/4\xi^2)\cdot(\varphi^2-1)^2, \tag{4}$$

where ξ is a capillary width that scales with the thickness of the diffuse interface. So from (2)-(4) it follows that the chemical potential can be specified as follows:

$$\nu = \frac{\alpha}{\xi^2}\left[\varphi(\varphi^2-1) - \xi^2\nabla^2\varphi\right] \tag{5}$$

The partial differential equation describing the evolution of φ is the convective Cahn-Hilliard equation:

$$\frac{\partial\varphi}{\partial t} + (\mathbf{u}\cdot\nabla)\,\varphi - \nabla\cdot(\Lambda(\varphi)\nabla\mu) = 0, \tag{6}$$

where for the nonlinear mobility $\Lambda(\varphi)$ which contributes much to the phase separation and usually is an important numerical parameter, we choose the following expression (cf. Badalassi et al, 2003):

$$\Lambda(\varphi) = \Lambda_c\cdot(1-\gamma\varphi^2)\xi^2. \tag{7}$$

Here $0\le\gamma\le1$. At $\gamma\to0$ the phase separation dynamics is controlled by bulk diffusion; in the opposite case $\gamma\to1$, the phase separation dynamics is controlled by interface diffusion.

Finally, combining (5), (6) and the *modified* Navier-Stokes equations for incompressible fluid, the system of model equations to be solved can be written as:

$$\rho\left(\frac{\partial\mathbf{u}}{\partial t} + (\mathbf{u}\cdot\nabla)\,\mathbf{u}\right) + \nabla p = \nabla\cdot\left[\mu\left(\nabla\mathbf{u} + (\nabla\mathbf{u})^T\right)\right] + \nu\cdot\nabla\varphi$$

$$\nabla\cdot\mathbf{u} = 0$$

+Eq.(5) +Eq.(6). (8)

The equilibrium profile is obtained by minimizing the free-energy functional F with respect to the variations of the function φ, i.e. simply solving for

$$\nu \equiv \delta F/\delta\varphi = 0,$$

where F is given by (2). In the case of one-dimensional interface the solution is (cf. Fichot, 2007)

$$\varphi = \pm\tanh[x/(2^{1/2}\xi)]. \quad (9)$$

Note that the equation above is locally true for any particular geometry of the interface in equilibrium and in many calculations presented in the paper the equation (9) has been used to provide the initial phase field over the model region. The interfacial surface tension (IFT) is introduced through the integral of the free-energy density across the interface; it can be shown that it relates the two above-defined model parameters α and ξ via the following useful equation:

$$\sigma = (2^{3/2}/3)\cdot(\alpha/\xi). \quad (10)$$

Dimensionless parameters

The dimensionless formulation contains as usual the Reynolds number, $Re=\rho u_i L/\mu$, appeared in the first equation of (8), but also the Cahn number, $Cn=L/\xi$, in the last term of this equation (cf. (12)). Here u_i is the typical velocity of injected fluid (usually water). Beside that the product of the Peclet number, $Pe=u_i\cdot L/(\Lambda_c\ Cn\cdot\sigma)$, and Cahn number arises in the last term of the equation (6). Other important parameters are the capillary number, $Ca=\mu_i\ u_i/\sigma$, and the viscosity ratio, $M=\mu_r/\mu_i$, i.e. the ratio of recovered (or initial, i.e. usually oil, in our applications) to injected fluid viscosity. Note that standard capillary number is defined in somewhat different manner via the injected fluid debit per unit area (or Darcy velocity), q_i , and includes frequently the contact angle at solid boundary, θ :

$$Ca^*=\mu_i\ q_i/\sigma,\ Ca^{**}=Ca^*/\cos\theta. \quad (11)$$

All these numbers may be important in defining typical flow regimes in a single and/or two-phase flow cases. The system of dimensionless equations reads as follows:

$$\begin{aligned} &Re\left(\frac{\partial\hat{\mathbf{u}}}{\partial t}+(\hat{\mathbf{u}}\cdot\nabla)\ \hat{\mathbf{u}}\right)+\nabla\hat{p}=\nabla\cdot\left[\hat{\mu}(M)\left(\nabla\hat{\mathbf{u}}+(\nabla\hat{\mathbf{u}})^T\right)\right]\\ &\qquad\qquad+\frac{1}{Ca\cdot Cn}\ \hat{v}\cdot\nabla\varphi\\ &\nabla\cdot\hat{\mathbf{u}}=0\\ &\frac{\partial\varphi}{\partial\hat{t}}+(\hat{\mathbf{u}}\cdot\nabla)\ \varphi-\frac{1}{Pe}\nabla\cdot\left(\hat{\Lambda}(\varphi)\nabla\hat{v}\right)=0 \quad (12)\\ &\hat{v}=\chi\left((\varphi^2-1)\cdot\varphi-Cn^2\nabla^2\varphi\right), \end{aligned}$$

where $\chi=3/2^{3/2}\approx1.06$, symbol "^" designates dimensionless quantity.

Test cases of model applicability and numerical performance

The successful test cases of the DI model included the following problems:

- the segregated stationary flow in plane and cylindrical 2D channels and their comparison to available analytical solutions;
- 2P flow patterns in plane channel without gravity;
- spurious velocity field around a droplet at rest;
- dynamics of the capillary meniscus advancement in tubes of constant and variable cross-sectional area;
- equilibrium two-phase configurations in 2D and 3D (*Bentheimer* rock sample) resulting from Cahn-Hilliard equation (spinodal decomposition),

and some others. Few advanced tests included 2D unstable displacement experiments modelling and analysis which is in part presented below; the *Bentheimer* sample absolute permeability estimation reported recently (*eg.* Bogdanov et al. 2012; some new results are also discussed here), and some of the tests are in course of finalization.

Single phase flow: influence of resampling.

Usually such a model addresses the determination of PM transport properties like absolute permeability closely related to PV geometry, connectivity etc. Recently we reported the influence of grid discretization size and other model parameters on the calculated permeability (Bogdanov et al. 2012). It was concluded that the coarse grid doesn't capture well the axial velocity profile, overestimate the resistance to flow in pores so that the permeability is lower for greater discretization. Also some results for different BC (no-slip, symmetry, lateral and full periodicity) obtained for the same grid have been presented. The results demonstrated regular increase of total debit from no-slip to fully periodic BC.

The general *resampling* effect on simulation results is similar to the discretization size but by a different reason. The coarser is the grain surface (and hence, the pore volume) characterization, the poorer porosity, connectivity and absolute permeability are obtained from computations. (It is obvious that increasing voxel volume at fixed bulk volume will lead to the loss of connectivity as demonstrated *eg.* in Figure 2(III) where image (linear) size unit is pixel). The table presented in Figure 2(II) summarizes the data for two resampling steps from the base case S of 125^3 voxels. The connected porosity (in %), the total grain surface (S_{gr}, in mm^2) and three diagonal components of the permeability tensor regularly decrease with increasing voxel size; the normalized variation of each quantity is illustrated in Figure 2(IV). Thus the grain surface and pore volume preserving procedures are necessary for more adequate description of the pore geometry at *resampling*.

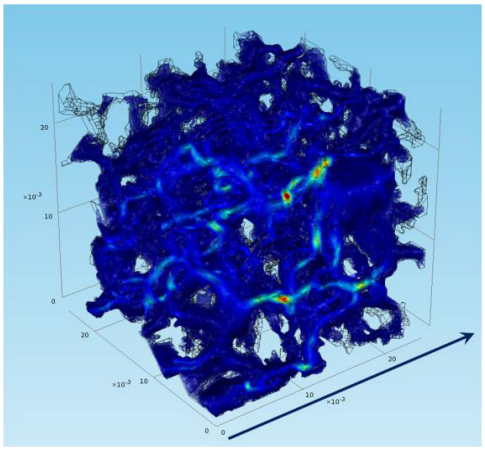

I

Sample	No. of voxels	Connected porosity	Grain surface
S	125^3	21.5	22.6
M	100^3	20.1	21.6
L	50^3	19.5	19.7
	K_X, D	K_Y, D	K_Z, D
S	3.41	3.34	3.99
M	2.74	2.76	3.26
L	2.24	2.53	2.78

II

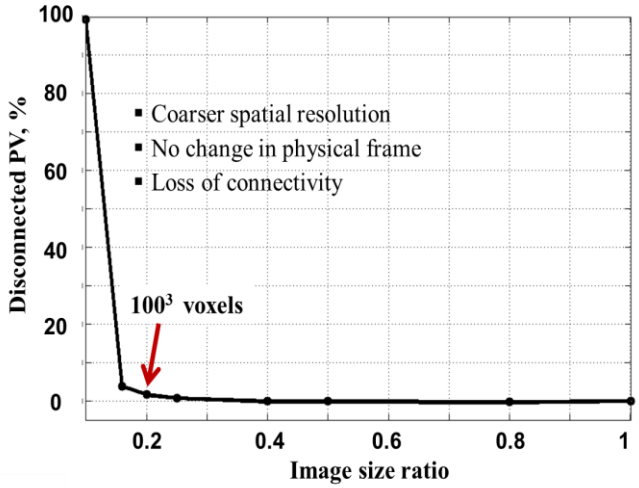

III

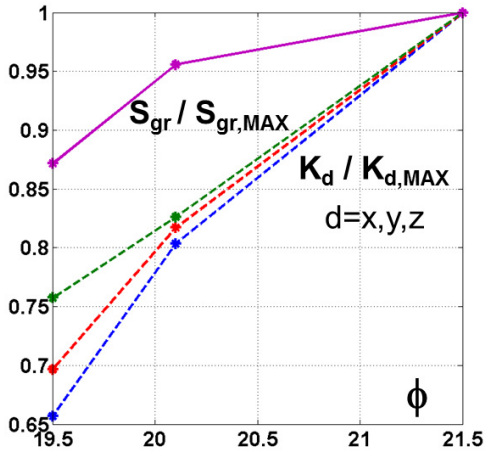

IV

Figure 2 *Influence of binarized pore volume resampling (i.e. increase of elementary voxel size at fixed sample volume) on geometrical and 1P transport properties of the sample shown in (I). (I) The total velocity field;(II,IV) summary of 2 resampling steps (M and L with respect to the base case S).*

Stationary and dynamic 2P flow configurations

Consider now some 2P flow cases. Remind first that the main objective of the PSM based on DNS approaches is the determination of fluids distribution and their dynamic redistribution inside a pore volume.
In the framework of DI approach the "real" flow regimes in different petroleum and environmental applications can be characterized by a range of typical variation for such dimensionless parameters as the capillary, Cahn and Peclet numbers (*Ca*, *Cn* and *Pe*). One more dimensionless parameter of importance is the contact angle θ which generally speaking may be considered as independent (and not just as a multiplier in conventional product $\sigma \cdot cos\theta$). The dimensionless model (12) has been extensively used for 2D and 3D cases related to both artificial and real permeable media geometry. Our very first systematic results on flow in a real medium were presented in Bogdanov et al. (2012).
One of the general observations of that initial period of work was that it seems possible that in the complex interplay resulting in 2P flow all factors are equally important so that any relatively important simplification in pore geometry model, fluids wetting and viscous properties, interfacial tension and/or hydraulic potential may lead to a non-adequate deviation from the "real" flow behaviour.
Even if this was just first observation which generally may be not precise, the pore scale models based on direct simulation approach can be really useful because of their better representativeness due to more precise description of the fluids dynamic distribution.

2½D flow in microfluidic channels

Recently Levaché and Bortolo (2014) described a series of lab experiments on unstable displacement of silicon oils by an aqueous solution in hydrophilic microfluidic channels of synthetic medium. Figure 3(I) illustrates one of the results for a rectangular pattern 40 by 15 mm at M=100. The rest of Figure 3 demonstrates the simulation results at different Ca^* and θ. (Remind that the definition of Ca^* (cf. (11) includes the IFT and not the contact angle factor, $cos\theta$, while Ca^{**} is based on the conventional product $\sigma \cdot cos\theta$ in static triple point consideration).
It turned out that the finger pattern was more sensitive to variation of θ (subplot IV vs. III in Figure 3) than Ca^* (subplot IV vs. II, same figure) within the range of tested parameters. Moreover their variations give qualitatively different results (*eg.* shape and total surface of fingers). In case θ (and Ca^{**}) increases, the flow pattern becomes more ramified and some number of local quasi-stagnant zones of nearly trapped oil (red phase) can be observed. Similar variation of Ca^{**} with decreasing IFT resulted in a quite different flow pattern (subplot II); this same pattern is reproduced on the two times larger domain representing half of the micromodel width (Figure 4(I)). So to effectively analyse this problem both parameters, i.e. θ and IFT, should generally be used independently.
Note that in this particular case the fingers geometry remains relatively stable which enables to estimate the typical finger width; this value is close to 1.7mm (about 5 grains shown in white in Figures 3 and 4). The detailed analysis of results reveals the localized and sporadic displacement behaviour illustrated in Figure 4(II). The total velocity field is not regular at all in space and time; it demonstrates, for instance, few local "breakthroughs" of injected fluid characterized by increased velocity inside a small group of channels (consisting, typically, of two or three channels, cf. red spots on Figure 4(II)) and stagnant flow zones (blue spots). The max to min ratio of the local velocity shown in this figure is 12.

3D flow in synthetic media

3D modelling of 2P flow in real media is a real challenge which up to now remains a problem of utmost technical complexity especially in case of natural flow regimes. By natural we imply here the regimes that can be observed at typical variation of main physical parameters in petroleum and environmental applications. Our work on 3D flow was started with problems of 2P flow in a regular packing of monodisperse spherical grains where both stable and unstable displacement took place (see Figure 5). The main objective of this study was to check the computational performance of the model.

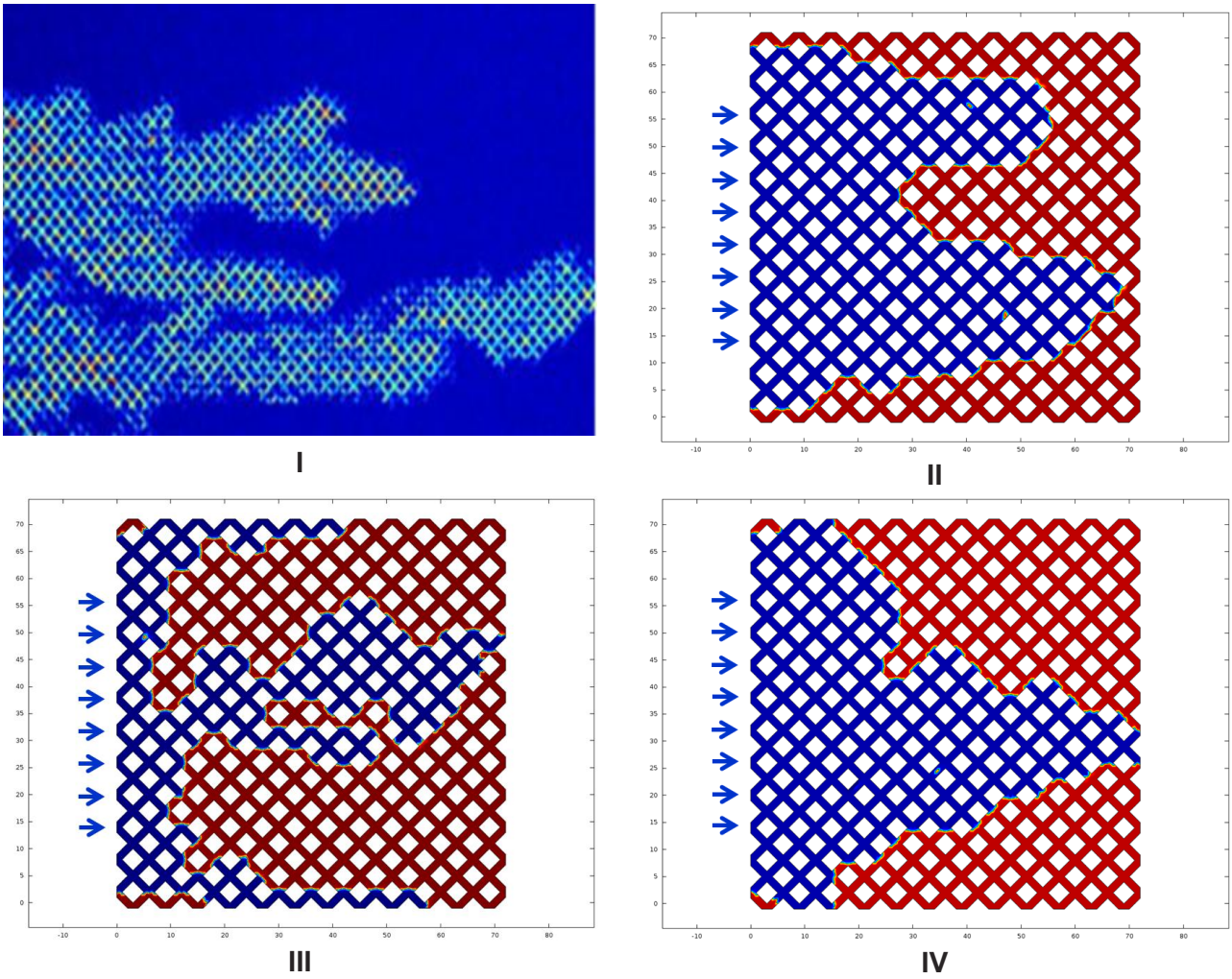

Figure 3 *One example of a simulation to experimental results comparison (Levaché 2013, cf. also Levaché and Bartolo 2014): (I) a part of rectangular pattern with unstable displacement (M=100) of the silicon oil; (II) simulation results at* $Ca^*=6.7\cdot10^{-5}$, $\cos\theta=0.87$; *(III and IV) simulation results for the same injected volume like (II) at* $Ca^*=2.7\cdot10^{-5}$ *(III and IV),* $\cos\theta=0.6$ *(III), 0.81 (IV). Injection took place at the same constant velocity through the pores indicated by blue arrows.*

The interesting applied aspect of such a modelling was the analysis of nearly singular configurations of flow related to unstable displacement. For instance, in case of such a displacement at high enough capillary numbers, i.e. with the typical size of fingers less than a channel width, the instability created a single finger configuration of 2P flow (Figure 5). The 3D field of variable φ illustrates the breakthrough of low-viscous fluid at drainage conditions.

It is difficult to imagine such kind of flow in real pore volume geometry where most probably the flow at this capillary number will lead to generation of separate blobs of fluid like those we could observe in 3D modelling of desaturation after imbibition (see the next subsection).

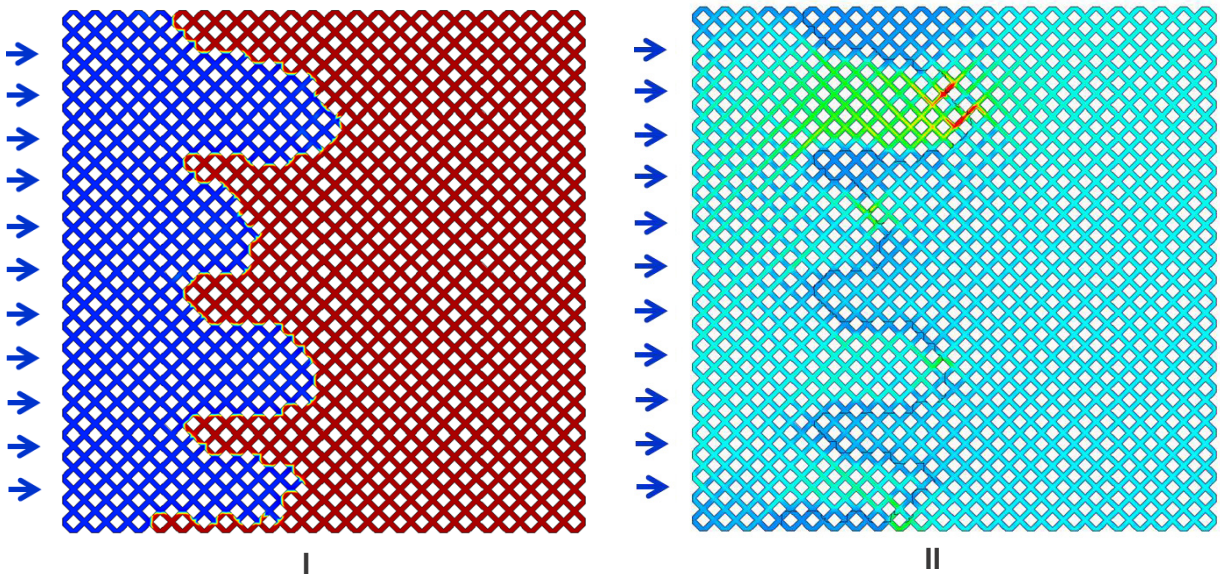

Figure 4 *(I) The similar case of finger pattern like in Figure 3 (eg. II or IV) but in a larger domain at* $Ca^*=3\cdot10^{-5}$, $\cos\theta=0.81$, $M=100$. *(II) The total velocity field, U(x,y), demonstrates the instantaneous map of the finger advancement;* $5\cdot10^{-5} \leq U \leq 6\ 10^{-4}$ *m/s.*

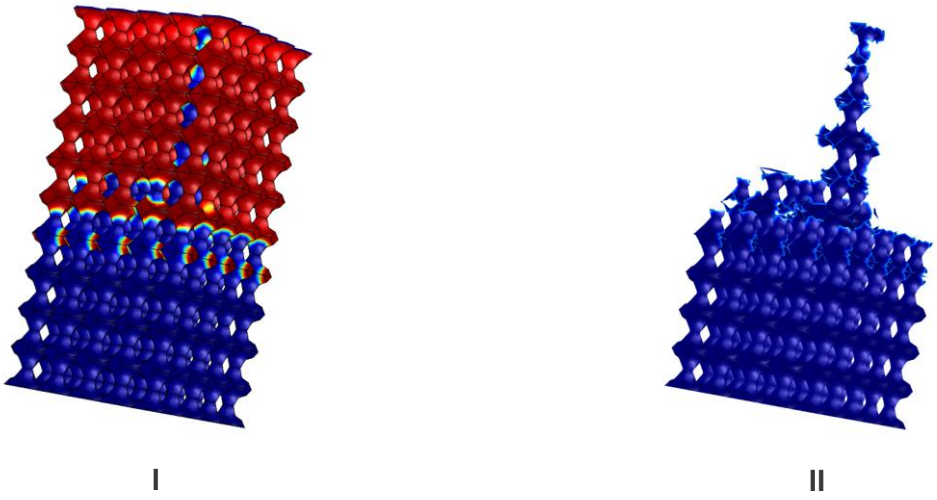

Figure 5 *(I,II) unstable displacement in regular pack of spherical grains at* $M=100$, $Ca^{**}=5\cdot10^{-4}$; *both fluids (I) and injected phase (II) instantaneous configurations.*

Imbibition and desaturation in a real medium

The locally dominating capillary forces at pore scale are responsible for the local mass exchange which is important phenomenon is many practical applications. Modelling this process in its dynamics in real pore volume may provide both better qualitative understanding and quantitative description of the 2P mass transfer. It seems relevant to emphasise that the dynamic of the interface shape and position in realistic geometry of pores is a key factor for such a modelling.

One of the first examples of the capillary imbibition in the imaged-based *Bentheimer* sample geometry is shown in Figure 6. A single pore at the input left side of the sample has initially been put in contact with wetting phase ("water"), the sample being initially saturated by non-wetting phase

("oil"). There was no pressure difference between the input (left) and output (right) sides during the whole process; the lateral sides were kept at the symmetry conditions (both for modified NS and CH equations).

Let's define the water "saturation", S_w, like the fraction of wetting phase in pore volume. Its variation with time indicates few local breakthroughs of the interface in the relatively narrow channels separated by periods of slow regular advancement; the end-point saturation is finally, $S_w^* \approx 0.78$ (Figure 6(IV)). Evidently the oil phase is completely disconnected at its final state (Figure 6(III). The simulation indicated that there exists a critical wetting angle for this sample (at zero pressure drop) which avoids the water blocking. This angle is close to $\theta=\pi/3$.

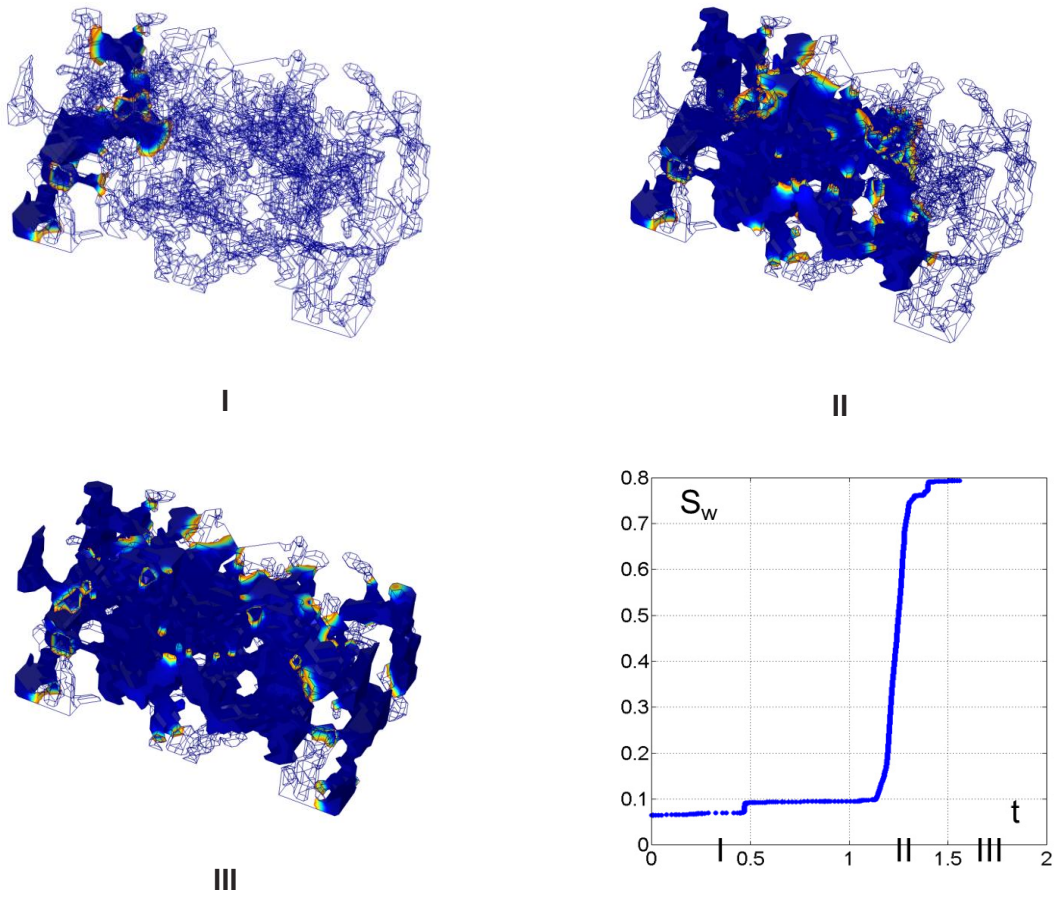

Figure 6 *(I,II,III) Pure imbibition in Bentheimer sample ($0.25 \cdot 10^6$ voxels) at $\Delta P = P_{in} - P_{out} = 0$, $M=1$, $\theta=\pi/3$, $\sigma=0.01$ N/m, $L_x=L/2$; the volume progressively occupied by wetting phase entering from the left side of sample is shown in bleu and phase interface in yellow; fraction of pore volume occupied by wetting phase (S_w) as a function of dimensionless time – in the right graph at bottom.*

In many petroleum applications (like, for instance, the chemical EOR) in order to estimate the oil recovery it is important to know the end-point oil saturation within a particular physical and chemical environment. We present here an example of pore-scale simulation of the desaturation due to the IFT diminishing (cf. Lake 1989) which can be a result of surfactant pre-injection at the final stage of imbibition (Figure 6(III)). This final fluid distribution after imbibition (which is equivalent to Figure 7(I)) has been taken as the initial conditions at this step; the water injection under the pressure drop ΔP=10 Pa has been imposed. The oil trapped in few pores is initially in disconnected form and thus in immobile state. At low enough IFT the oil was swept out from some of these pores as it can be readily viewed from comparison of subplots I and II in Figure 7. Note in particular that the displacement after the mobilization of the oil trapped in the pore at left bottom corner (subplot I) passed through the

formation in series of three independent blobs of oil leaving the sample through the output end at the right side. This is the main mechanism of how the desaturation took place in the sample.
The dimensionless water debit variation with time (Figure 7(III)) demonstrates the gradually increasing flow which is due to the oil sweep from a part of pore volume. Note also that being initially discontinuous the oil phase flows out of sample as a dispersed phase with few separate droplets. The resulting new oil saturation established after about 2PV injected ($t \approx 1$) is $S_o^{**}=1-S_w^{**}\approx 0.1$. Finally, the desaturation curve for the *Bentheimer* sample under consideration after imbibition at $M=1$ is depicted in Figure 7(IV).

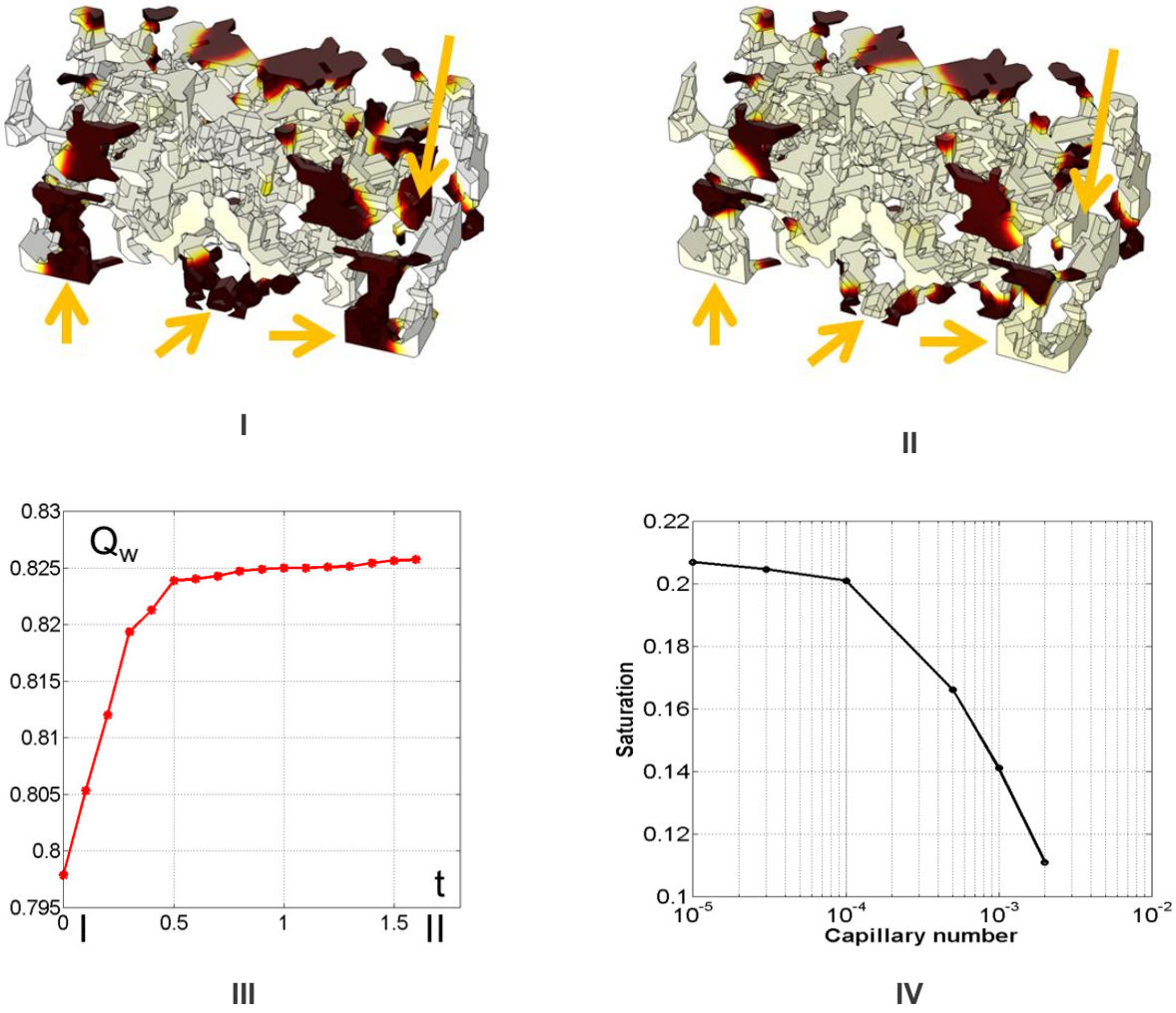

Figure 7 *The desaturation after imbibition at $Ca^*=10^{-3}$ via the water injection from the left side of the sample at given pressure drop (10 Pa): (I) imbibition end-point configuration; (II) desaturation end-point configuration; (III) water debit variation with time; (IV) summary of desaturation (after imbibition) at different capillary numbers for the Bentheimer sample.*

Conclusions

- The methodology of image based direct numerical simulations of pore-scale flow modelling development is addressed and presented in some detail. This includes a number of steps like the construction and processing of the image-based geometry of real pore volume, efficient numerical

model adaptation (including grid and special solvers) and necessary testing procedure which is not straightforward.

- As a main objective of the pore-scale modelling based on a direct numerical simulation approach we consider the determination of dynamic fluids distribution and their behaviour inside a "real" pore volume. The diffuse interface approach is a suitable means for direct numerical modelling of 2P flow.
- The pore volume modifications that can be put in place to reduce the simulation time are acceptable within certain limits. However, volume and surface preserving procedures are necessary for successful resampling of real geometries.
- The interplay of capillary domination at local scale and complex geometry of pore volume implies that the contact angle can be an independent model parameter in some situations (dynamic viscous fingering) etc.
- Simulation of a typical desaturation curve supplemented the successful tests lists for the methodology.

This paper has therefore demonstrated a number of useful qualitative applications for DNS: nevertheless, as a concluding remark, we reinforce the point that the application of this technology for oil and gas industry is not straightforward, at least at quantitative or predictive level, and that numerous challenges remain to be tackled.

Acknowledgement

TOTAL SA is gratefully acknowledged for sponsoring CHLOE's research activities. We wish to thank F. Guerton (LFC-R, University of Pau) for valuable discussions and collaboration during the stay of J. Kpahou at CHLOE.

References

Adler, P.M., Jacquin, C. G. and Quiblier, J. A. [1990] Flow in simulated porous media. *International Journal of Multiphase Flow*, **16**(4), 691-712.

Badalassi, V., Cenciceros, H. and Banerjee, S. [2003] Computation of multiphase system with phase field models. *Journal of Computational Physics*, **190**,371-397.

Bear, J. [1988] *Dynamics of fluids in porous media*, Dover Publications, Inc., New York.

Blunt, M.J., Bijeljic, B., Dong, H., Gharbi, O., Iglauer, S., Mostaghimi, P., Palusznya, A., and Pentlanda, C. [2013] Pore-scale imaging and modeling. *Advances in Water Resources*, **51**, 197–216.

Bogdanov, I. Kpahou, J. and Guerton, F. [2012] Pore-scale single and two-phase transport in real porous medium. *13th European Conference on Mathematics in Oil Recovery, ECMOR XIII, 10 - 13 September, 2012, Biarritz, France*.

Cahn, J.W., Hilliard, J.E. [1958] Free Energy of a Nonuniform System. I. Interfacial Free Energy, *Journal of Chemical Physics*, **28**(2), 285-267.

Fichot, F., Meekunnasombat, P., Belloni, J., Duval, F., Garcia, A. and Quintard, M. [2007] Two-phase flow in porous media: prediction of pressure drops using a diffuse interface mathematical decription. *Nuclear engineering and design,* **237** 1887-1898.

Fourie, W., Said, R., Young, Ph., Barnes, D.L. [2007] The Simulation of Pore Scale Fluid Flow with Real World Geometries Obtained from X-Ray Computed Tomography, *Proceedings of the Boston COMSOL Conference* , Boston, MA.

Jacqmin, D. [1999] Calculation of two-phase Navier-Stokes flows using phase field modeling, *Journal of Computational Physics*, **155**, 1-32.

Kalaydjian, F. [1990] Origin and quanification of coupling between relative permeabilities for two phase flows in porous media. *Transport in porous media*, **5**, 155-169.

Koroteev, D., Gurpinar, O., Dinariev, O., Berg, S., van Kruijsdijk, C., Evseev, N., de Jong, H., Klemin, D., Armstrong, R., Nadeev, A., Myers, M. T., Safonov, S. and Hathon, L. [2013] Direct hydrodynamic simulation of multiphase flow in porous rock. *International Symposium of the Society of Core Analysts held in Napa Valley, California, USA, 16-19 September, 2013*.

Lake, L. W. [1989] *Enhanced oil recovery*. Prentice-Hall, New York.

Levaché, B. [2013] Personnalk communication.

Levaché, B. and Bartolo, D. [2014] Revisiting the Saffman-Taylor experiment: imbibition patterns and liquid-entrainment transitions. arXiv:1404.2397v1 [cond-mat.soft].

Wildenschild, D. and Sheppard, A.P. [2013] X-ray imaging and analysis techniques for quantifying pore-scale structure and processes in subsurface porous medium systems. *Advances in Water Resources*, **51**, 217-246.